Geophys. Astrophys. Fluid Dynamics, Vol. 83, pp. 195–231
Reprints available directly from the publisher
Photocopying permitted by license only

NUMERICAL STUDIES OF SMALL ISLAND WAKES IN THE OCEAN

DAVID E. DIETRICH[a], MALCOLM J. BOWMAN[b], CHARLES A. LIN[c] and ALBERTO MESTAS-NUNEZ[a]

[a]*Center for Air Sea Technology, Mississippi State University Stennis Space Center, MS 39529*
[b]*Marine Sciences Research Center, State University of New York Stony Brook, NY 11794*
[c]*Department of Atmospheric and Oceanic Sciences, and Centre for Climate and Global Change Research, McGill University, Montreal, PQ, Canada H3A 2K6*

(Received 17 October 1995; In final form 22 April 1996)

Two and three-dimensional oceanic flows around small islands patterned after Barbados, W.I. (13° 10′ N latitude: 59° 30′ W longitude) were modeled numerically to investigate island wake effects. The two-dimensional simulations closely agreed with laboratory flows, for both attached and shedding wake regimes. As expected, results for a flat bottom confirmed that the Coriolis terms strongly affect pressure but not the flow.

For idealized, yet typical incident flow speeds, water column stratification, island topography and appropriate Coriolis terms, three-dimensional simulations readily produced elongated wake patterns, dominated by surface intensified von Karman–like vortices. Effects of grid resolution, viscosity, bathymetry, and Coriolis forces on wake characteristics were studied. For islands with typical bottom slopes, realistically small horizontal eddy diffusivity has a minor effect compared to bottom drag in generating vorticity. Near-shore bathymetry (viz., the absence or presence of a continental shelf surrounding the island) plays a major role in determining the scale, intensity, and shedding period of the vortices. The addition of a 15 km wide continental shelf around the island increased the shedding period by 67%, while reducing the Coriolis force by 50% reduced the period by only 14%. Although observational data is sparse, inferred flow patterns do show von Karman-like structures near Barbados, even if eddies are not located exactly as expected. The numerical computations demonstrate that shedding eddy wakes are easily generated, and lend encouragement to the further search for organized wakes downstream of the island.

Keywords: Oceanic flows; island wakes; bathymetry

1. INTRODUCTION

Fluid flow past steep obstacles is a complex phenomenon, a problem of considerable interest in geophysical fluid dynamics. The literature on rotating tank experiments can be conveniently grouped into: steady versus non-steady (i.e., accelerating or oscillating) wakes (e.g., Lugt and Haussling, 1974); homogeneous versus stratified flows (e.g., Brighton, 1978); non-rotating flows versus rotating f-plane (e.g.,Boyer and Kmetz, 1983; Walker and Stewartson, 1972) and β-plane flows (e.g., Boyer and Davies, 1982); circulation around cylindrical versus other shapes of obstacles, such as right circular cones, cosine bells, hemispheres, spheroids, and ellipsoids (e.g.,Brighton, 1978).

Boyer (1970) carried out a series of laboratory experiments of slightly viscous homogeneous flow past a circular cylinder in a rotating system. The flow was found to be fully attached in the limit of zero Rossby number. However, separation occured for small but finite Rossby numbers. Using quasi-geostrophic theory, Walker and Stewartson (1972) derived a criterion for flow separation which depends on the ratio of the Rossby number and the square root of the Ekman number. Merkine and Solan (1979) re-examined the problem and included higher order Rossby number effects. Further theoretical studies by Merkine (1980) and laboratory experiments by Boyer and Davies (1982) demonstrated the effect of the variation of the Coriolis parameter with latitude, the β-effect. The effects of stratification were examined in later studies by Brevdo and Merkine (1985) and Merkine (1985).

Relatively few observations and numerical studies of oceanic vortex streets behind islands located on the continental shelf or open ocean have been published. Barkley (1972) reported on an oceanic wake downstream of Johnson Atoll in the tropical Pacific Ocean which resembled a von Karman wake (von Karman and Rubach, 1912). Three wake eddies were observed, spaced about 80 km apart, and with a shedding period of about four days.

A spectacular wake of well organized spiral cyclones was observed in the ocean near Grand Bahama Island, western Atlantic Ocean, by Fu and Holt (1982) using Seasat synthetic aperture radar images of sea surface roughness. A string of at least seven cyclones separated off the southwestern tip of the island and east of the Gulf Stream (inci-

dentally Grand Bahama Island is similar in size to Barbados, discussed in this paper) and migrated with the mean flow, curling counter-clockwise in a large circular arc south of the island.

Heburn *et al.* (1982) and Kinder *et al.* (1985) numerically studied the observed widespread eddy activity in the Caribbean Sea using a two-layer model. They focused on wake interactions among prescribed inflows through ports patterned after major island passages. They related the eddy activity to shear instabilities and interactions among the prescribed inflow jets.

Bowman *et al.* (1983) observed a train of cyclonic eddies streaming away from the Kahurangi Shoals, a mid-shelf bluff obstacle on the western shelf of the South Island of New Zealand. Strong upwelling within the eddies stimulated enhanced primary production, supporting a tightly coupled food chain and a productive squid fishery. Chiswell (1993) studied the generation of vorticity in the vicinity of the shoals, and found that bottom friction on the outer flank of the shoals was responsible for the generation of cyclonic vorticity.

Wolanski (1988) reported on observations and barotropic model results for tidal flows around Rattray Island, located on the Great Barrier Reef, northeast Australia. He noted that vertical circulations were significant in the wake eddies and shear zones either side of the island. Earlier, von Riegels (1938) and Wolanski *et al.* (1984) proposed that island wakes in shallow seas are controlled by Ekman layer effects arising from the interaction of the flow with the gently sloping bottom around the island rather than by the effects of horizontal viscosity.

Deleersnijder *et al.* (1992) applied a sigma-coordinate model to the tidal flow around Rattray Island. Although the model was limited by insufficient resolution, two counter-rotating eddies developed in the wake, with upwelling occurring in the eddy centers. Upstream of the island, strong downwelling was found. Further discussions of shallow sea wakes and island effects can be found in Hogg (1980), Pingree and Maddock (1980); Falconer *et al.* (1985,86a,b); Wolanski (1986); Black and Gay (1987); Ingram and Chu (1987); Tomczak (1988); Wolanski and Hamner (1988); Deleersnijder *et al.* (1989); Signell and Geyer (1991); Davies and Mofor (1990); Middleton *et al.* (1993); and Pattiaratchi (1994).

Chapman and Haidvogel (1992) modeled flow past a steep seamount in the deep sea (approximating Fieberling Guyot), but focused

on Taylor cap formation rather than eddy shedding. In agreement with observations, they were able to generate conical caps only for very limited range of the Rossby number $0 < Ro < 0.1$.

Schar and Smith (1993a,b) numerically modeled a single layer of shallow water flowing past three-dimensional circular, gently sloping topography in the absence of surface stress and rotation for both steady left-right wake symmetry (Schar and Smith, 1993a) and for von Karman-type oscillating wakes (Schar and Smith, 1993b). The intent was to discover whether the pseudo-inviscid shallow-water theory of vortex shedding was applicable to atmospheric mixed layer flows under pronounced inversions (as observed in atmospheric vortex streets behind mountains), and with the theory of vortex shedding in two-dimensional homogeneous and atmospheric flows (Smith, 1989). Good agreement was found between the numerically computed Strouhal number and the observations of atmospheric eddies formed behind a number of mountainous islands (see review by Chopra, 1973 and Atkinson, 1981).

Prompted by observations of island wakes and headland flows on the continental shelf (Pattiaratchi *et al.*, 1986), Denniss and Middleton (1994) numerically studied the relative effect of bottom friction and horizontal viscosity and claimed that a ratio of scales of the nonlinear and bottom friction terms often govern the nature of recirculation in the lee of coastal islands, instead of the eddy Reynolds number based on horizontal eddy viscosity alone.

Bowman *et al.* (1994) and Stansfield *et al.* (1995) reported observations of eddies close to the island of Barbados, West Indies (13° 10′ N; 59° 30′ W; Fig. 1) based on geostrophic calculations made on a dense set of conductivity-temperature-depth (CTD) data and hull-mounted acoustic doppler current profiler (ADCP) records.

In both 1990 and 1991, meanders and eddies were observed near the island (Figs. 2, 3), whose scales and senses of rotation were consistent with a von Karman-type wake. Because of logistical constraints, the surveys did not extend far enough to sea to map the entire wake structures (the two surveys shown took a week of cruising each; longer surveys also raise questions relating to synopticity). Since the upstream ambient flow was non-uniform, it was not possible to present a simple explanation of the observed circulation. For example in 1990, a large anticyclonic eddy originating in the Brazilian Current retroflec-

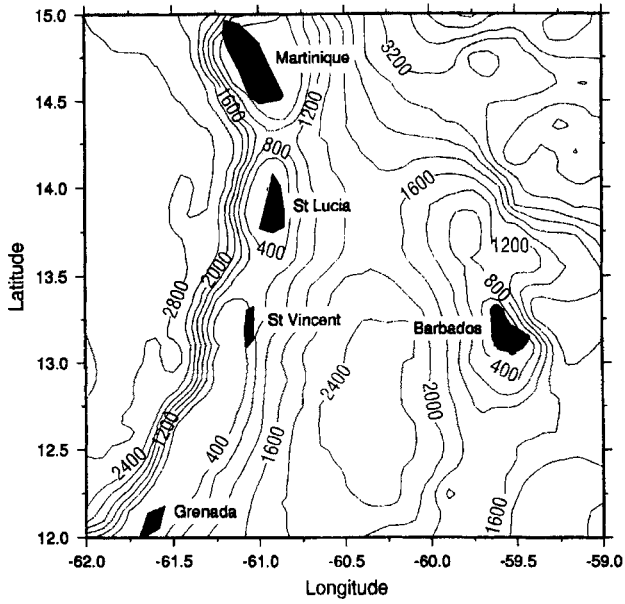

FIGURE 1 Locator map showing the island of Barbados and selected islands in the Lesser Antilles island chain. Depth contours are in m.

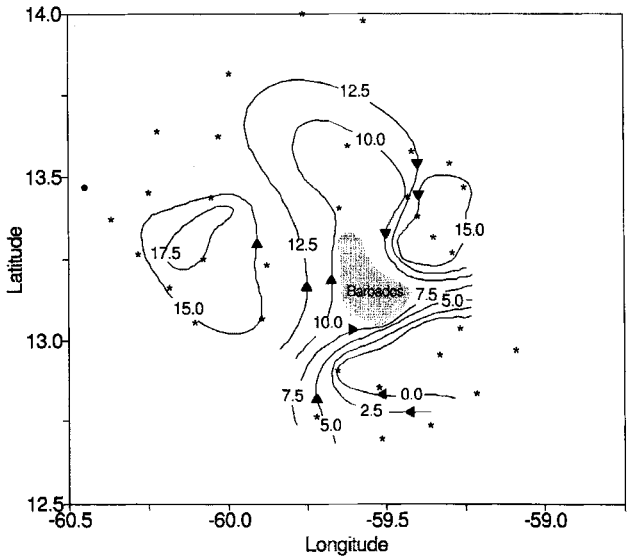

FIGURE 2 Relative topography (cm) of the sea surface with respect to 500 dbar for 1990, leg 2 (May 5–12). Values are actually negative, but the sign has been omitted for clarity. The stars represent CTD stations (from Bowman *et al.*, 1994).

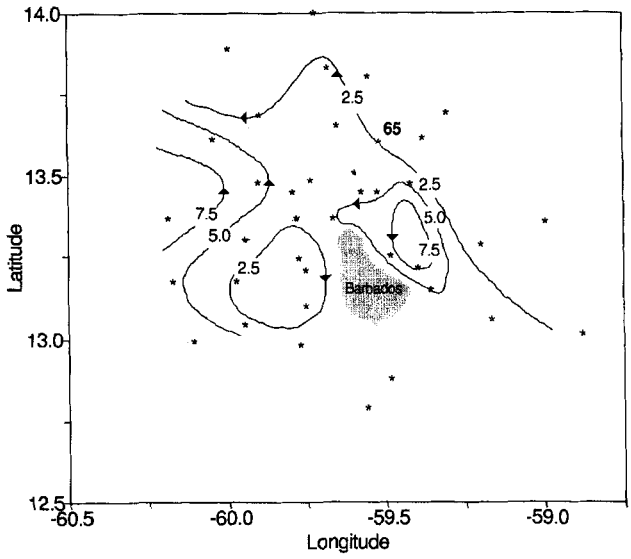

FIGURE 3 Relative topography (cm) of the sea surface with respect to 500 dbar for 1991, leg 2 (April 25 to May 2). Values are actually negative, but the sign has been omitted for clarity. The stars represent CTD stations (from Bowman *et al.*, 1994).

tion region was observed colliding with the island, causing major disruptions.

In this paper we numerically model and analyze organized oceanic wakes around small, isolated islands patterned after Barbados. The intent is not to attempt to model the observations reported by Bowman *et al.* (1994) and Stansfield *et al.* (1995) per se. Rather, we interpret the results of generic simulations with idealized topography to help explain the underlying physics of island wakes, and compare two and three-dimensional flows for obstacles of similar scale, flow velocities, stratification and latitude to that at Barbados. A numerical study of three-dimensional circulation patterns over the accurate bathymetry around Barbados is underway, and will be reported elsewhere.

Four scenarios were studied: i) two-dimensional homogeneous flow past a 50 km diameter cylindrical obstacle in a non-rotating ocean of uniform depth; ii) two-dimensional homogeneous flow past a 50 km diameter cylindrical obstacle in a rotating f-plane ocean (at latitude

13° N) of uniform depth; iii)three-dimensional flow past an elliptical Gaussian bell shaped island approximating the form and latitude of Barbados, with a far field uniform depth of 2000 m and realistic stratification; and iv) three-dimensional flow past a similar Gaussian bell shaped island, but surround by a 15 km wide, nearly flat continental shelf positioned at about 100 m depth below mean sea level. Below 1200 m, the bottom profiles were essentially identical to case ii) above.

Several basic aspects of the physical problem are discussed in Section 2. The model is briefly described in Section 3. The various runs are described in Section 4, and the results discussed and summarized in Section 5.

2. BACKGROUND

Time dependent vortices can occur in the wakes formed behind isolated obstacles, even with steady upstream conditions. In unstratified fluids, vortices develop from flow instabilities once the Reynolds number Re exceeds a critical value (which depends on island size and shape, upstream flow distribution, and fluid viscosity). Vorticity is generated in boundary layers on the sides of the island, which feeds into two attached eddies located behind the island, and which eventually separate and drift downstream with the ambient flow.

In laboratory flows, for $0 < Re < 100$, two elongated filamentary vortex lobes occur in a steady wake, one emanating from each side of the body. They contain vortical fluid that originates near the corresponding upstream stagnation point. For higher Re, these filaments are unstable to small perturbations, resulting in continual breaking away of boundary layer vortices which propagate downstream. There is a characteristic period between these separations as shedding alternates from one side of the island to the other with opposite sense of rotation (e.g., see Lin, 1954)

One might consider the wake behind an idealized, isolated island with finite surrounding topography to be similar to that formed behind a cylindrical obstacle, if the smoothly increasing depth profile were approximated as a series of cylindrical cross-sections, increasing in diameter with depth. The question then arises as to whether the

flow could be considered as a superposition of two-dimensional wakes, one for each depth. Such wakes could be derived from two-dimensional vorticity dynamics, applied independently at each depth level.

For geophysical flows in which buoyancy and rotation can be important, such a two-dimensional description would be invalid since the vertical variations of the horizontal vortex flow component would require geostrophic adjustment and quasi-geostrophic dynamics which involve vertical motions. These vertical motions would cause vortex stretching which in turn could substantially affect the vortex street. On the other hand, it is well known that low Rossby number geophysical flows can form Taylor columns and caps without eddy shedding (e.g., Chapman and Haidvogel, 1992). This could make flow around a circular island behave like flow around a cylinder with diameter equal to the island diameter at depth in the low Rossby number limit. A two-dimensional description might then be qualitatively valid.

During the spin-up phase of runs with low horizontal viscosity (high Reynolds number), the wake first elongates with a reverse flow directed back towards the island along the wake axis. This leads to an instability that destroys the symmetry of the wake. Schar and Smith (1993b) showed that the most unstable normal mode relies on a positive feedback mechanism located on the shearlines on either side of the wake. A frequency selection criteria for absolute instabilities in slowly varying shear flow successfully predicted the growth rate of the most unstable normal mode. The nonlinear evolution of this instability breaks up the steady wake into an oscillating von Karman vortex street. Each vortex exists as a coiled stream of fluid derived from hydraulic jumps of alternating strength located on the two flanks of the obstacle.

Schar and Smith (1993b) also noted that the remarkable geometric similarity between pseudo-viscous wakes in three-dimensional flows around sloping obstacles, and wakes in two-dimensional viscous flows, is due to two causes. In two-dimensional flows the vorticity is attributed to the no-slip condition at the surface of the obstacle and viscous diffusion of vorticity away from the source regions into the wake. In the three-dimensional model, the vorticity is produced in shallow waters (Ekman layers for rotating flows) lying on the sloping

flanks of the island, where the local Froude number exceeds unity and hydraulic jumps are formed. These unsteady jumps undergo a periodic lateral movement back and forth accompanied by large variations in their strength, and are closely related to the generation of the individual vortices.

The second similarity is due to the fact that the advection of vorticity from the generation regions into the wake eddies is identical in both two and three-dimensional situations. The nature of this vorticity advection is responsible for both the linear shear instability and the establishment of the vortex street itself.

3. THE NUMERICAL MODELS

The recently developed DieCAST model (Dietrich-Center for Air Sea Technology model (Dietrich *et al.*, 1993; Dietrich and Ko, 1994) is a three-dimensional, incompressible, primitive equation, low dissipation ocean model based on a modified (semi-collocated) Arakawa "a" grid. It incorporates the standard hydrostatic and Boussinesq approximations. It also uses a rigid-lid approximation, which gives nearly the same results as free surface models for the main energy containing ocean general circulation components.

The rigid-lid pressure algorithm presently in the DieCAST model was first introduced into the SOMS model (Sandia Ocean Model System. Dietrich *et al.*, 1987; Dietrich *et al.*, 1990 Dietrich, 1992) which uses a modified Arakawa "c" grid. It is worth noting that a similar pressure algorithm was applied to the Bryan-Cox model which uses an Arakawa "b" grid (Bryan, 1969; Cox, 1984) by Dukowicz and Malone (1992). Dietrich and Ko (1994) have shown that both the CAST and SOMS models have similar efficiencies and give very similar results.

The governing equations are

$$u_t = -p_x/\rho_o + fv - \nabla\cdot(u\mathbf{V}) + \nabla\cdot A_h\nabla u + (K_h u_z)_z, \tag{1}$$

$$v_t = -p_y/\rho_0 - fu - \nabla\cdot(v\mathbf{V}) + \nabla\cdot A_h\nabla v + (K_h v_z)_z, \tag{2}$$

$$T_t = -\nabla\cdot(T\mathbf{V}) + \nabla\cdot A_v\nabla T + (K_h T_z)_z, \tag{3}$$

$$p_z = \varepsilon g T, \qquad \nabla \cdot \mathbf{V} = 0. \tag{4,5}$$

The symbols u, v, p, T, t denote the zonal (x) and meridional (y) velocities, pressure, temperature, and time, respectively; V is the three-dimensional velocity field including the vertical (z) motion. Subscripts x, y, z, t denote partial differentiation with respect to space and time. The variable Coriolis parameter is f, while ε, g, ρ_0 are the coefficients of thermal expansion, the gravitational acceleration, and a reference density respectively; A_h, A_v, K_h, K_v are the eddy diffusivities for momentum and heat in the horizontal and vertical planes.

Equations (1) and (2) are the horizontal momentum equations, (3) is the temperature equation, (4) is the hydrostatic relation, while (5) is the continuity equation for a Bousinessq fluid.

The DieCAST and SOMS models use z-level vertical coordinates. Seabed dissipation effects are modeled by bottom drag combined with a staircase approximation of the bathymetry, similar to the Bryan-Cox model (Bryan, 1969; Cox, 1984). No other geometric approximations (such as topographic filters or amplitude limits) are used or required for stability.

To avoid the need for elliptic rigid-lid pressure solvers that solve island and irregular geometry directly, our models use a "swamp layer" approach (Zuur and Dietrich, 1990). This approach treats land locations as having one layer of highly viscous water, such that it never accelerates significantly from rest. In practice, the initial flow at each time step is set to zero in top layer locations over land, equivalent to assuming an infinite bottom drag coefficient. However, the time stepping is carried out as if there were actually one layer if water over land. Except for a very brief initial transient during the first few time steps, this results in maximum velocities of water over land being orders-of-magnitude smaller than the velocities in the "true" water regions, and is thus a good approximation (see Appendix I).

4. NUMERICAL RESULTS

4.1. Two-Dimensional Wakes Behind an Infinite Cylinder

To explore the DieCAST model's usefulness in island wake problems, both the classical two-dimensional steady wake with left-right symme-

try and the von Karman vortex street formed behind an infinite vertical cylinder were generated. A reduced one-layer version of the model, with free-slip bottom condition, zero wind stress, constant horizontal eddy viscosity, and a uniform upstream velocity of 0.4 ms^{-1} was used to examine the wake behind a 50 km diameter obstacle (representative of the diameter of Barbados at about 100 m below mean sea level). Runs without rotation are presented in Section 4.1.1. Runs with Coriolis forces present are discussed in Section 4.1.2.

The cylinder was located along the central axis of a 400 km by 400 km square channel, centered 100 km from the upstream boundary. The channel side walls had zero tangential stress, but were assumed rigid. After modifying the outflow so that its total volume flux matched the inflow, as required by incompressibility, a Neuman outflow condition was applied.

The rigid-lid surface pressure calculation maintains a non-divergent one layer flow exactly, just as it maintains an exact non-divergent barotropic (vertically integrated) horizontal velocity flow in three-dimensional simulations. With more than one layer, horizontal divergence occurs in the baroclinic (deviation from vertical average) horizontal velocity components, thus admitting vortex stretching dynamics (Dietrich *et al.*, 1987).

An equivalent approach would be to use a non-divergent barotropic vorticity equation to determine the streamfunction. In such an approach, the streamfunction value on the island boundary becomes time dependent in the vortex shedding regime. Its determination would require special computations that are not well suited to vector computers and can be poorly conditioned when applied to the vertically averaged flow in real oceans (Dukowicz and Malone, 1992). However, our model experiments simulate truly two-dimensional flows that cannot be realized exactly in Lin's experiments because of bottom boundary layer effects which interact with the sidewall (Stewartson) layers.

4.1.1. Low and Critical Reynolds Number Flows Without Rotation

The DieCAST model was run at two spatial grid sizes (5.0 and 2.5 km, corresponding to 80×80 and 160×160 cells, respectively) to test for adequate resolution. Results were then compared with each other and

with a well known laboratory-observed two-dimensional subcritical wake structure (Taneda, 1956). The model was run with horizontal eddy viscosity chosen to be $A_h = 512$ m^{2}s^{-1}, upstream velocity $V_o = 0.4$ ms^{-1}, and island diameter $d = 50$ km. These values give $Re = V_o d/A_h = 39$, which is the same value reported by Taneda, although of course he used molecular viscosity in his estimate of Re. Figure 4 illustrates the numerically derived streamlines with those photographed during the laboratory experiments. The streamfunctions show a remarkable similarity, which lends credence to the model's ability to generate realistic two dimensional wakes.

[Note: in model output contour plots, because of the different ranges encountered in the various variables, we have established the

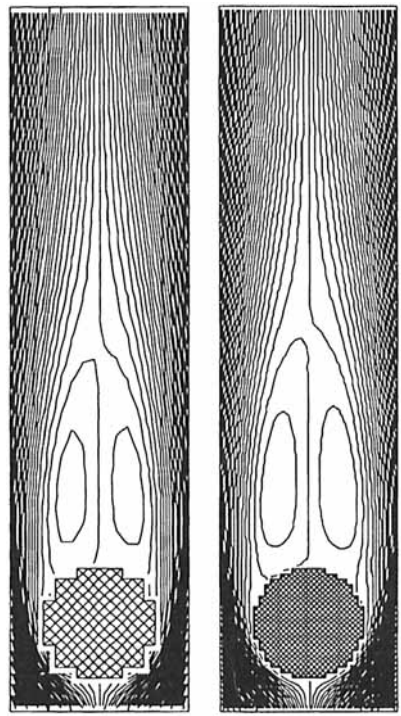

FIGURE 4 Streamlines for attached steady flow around a 50 km dia., two-dimensional cylinder using the DieCAST model. All runs were made at $Re = 39$.
a) 5.0 km resolution (left panel). [0, 1.6×10^5, 800 (m^2 s^{-1})];
b) 2.5 km resolution (center panel) [0, 1.6×10^5, 800 (m^2 s^{-1})].

FIGURE 4c Laboratory observations of Taneda, 1956 (right panel).

following convention. Each figure caption contains the string (minimum, maximum, contour interval). In many, but not all plots, there are ten contour levels displayed. The number of levels is adjusted to most clearly show salient features].

Figure 5 illustrates contours for relative vorticity for the two runs shown in Figure 4. Vorticity, being a second derivative of the streamfunction, requires higher resolution to converge. Its convergence requires the resolution of extremely thin boundary layers whose thickness l is such that the boundary layer-scaled Reynolds number $Re' = (V_o l/A_h)$, is of order unity. This means, for example, that the grid interval Δx must be at most about 1/40 of the island size to resolve the boundary layer near the upstream stagnation point when $Re \sim 40$, say. Until the somewhat thicker downstream vorticity boundary layer is resolved, one would expect the maximum free

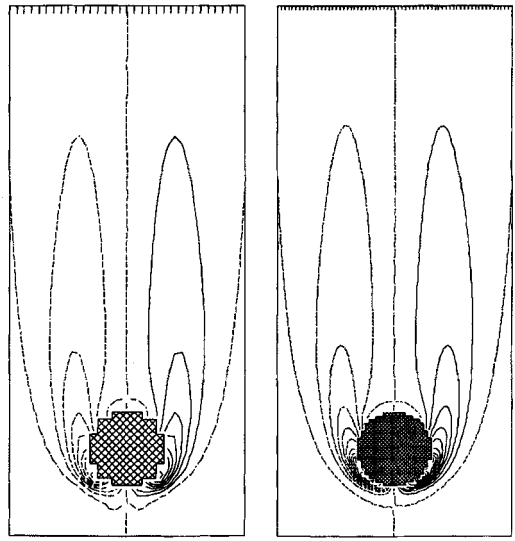

FIGURE 5 Steady state vorticity (end of week 1) for the flows shown in Figure 4. Both runs were made at $Re = 39$.
a) 5.0 km resolution (left panel) [$-40.7, 40.7, 8.14$ (rad wk^{-1})];
b) 2.5 km resolution (right panel) [$-59.3, 59.3, 11.9$ (rad wk^{-1})].

stream velocity to remain relatively constant while the maximum vorticity roughly doubles each time the resolution is doubled.

Even with 2.5 km resolution, Δx is twice as large as needed to well resolve the upstream boundary layer according to the above criterion. Nevertheless, Figure 5 shows that the vorticity from these calculations was reasonably well converged.

The same test was run with the SOMS model. Comparison of vorticity plots such as illustrated in Figure 5 were essentially similar (not shown); very small differences between results from the two models were due only to truncation errors, so all results presented in this paper are taken from the DieCAST model.

The critical range of Reynolds numbers which the wake changed from a stable, steady flow with left-right symmetry to a shedding, time-dependent vortex street was determined with the 25 km model with the same geometry and ambient flow as above. The model was spun up from rest with an initial value of $A_h = 250$ m^{2}s^{-1} (corresponding to $Re = 80$). With the model running, A_h was very slowly

decreased (through multiplication of A_h by a factor of 0.9999 at each time step) down to a final value of $A_h = 44$ m^{2}s^{-1} at day 120 (corresponding to $Re = 450$). This procedure generated first the steady attached wake, but once a critical value of Re was reached, the wake slowly evolved from time-invariant, attached counter-rotating eddies, to attached but oscillating eddies, then to a fully developed von Karman vortex street.

The first transition, as indicated by the appearance of asymmetry in the vorticity field (defined as when the ratio of the magnitudes of the maximum and minimum vorticity in the centers of the two eddies differed from unity by more than 10^{-6}) first occurred when A_h fell below 175 m^{2}s^{-1} (corresponding to $Re = 114$). This would happen about day 25.

The attached eddies then began to oscillate in a quasi-linear fashion with a period ~ 10 days until a finite amplitude was reached at about day 64 (with $A_h = 100$ m^{2}s^{-1}, corresponding to $Re = 200$). This is illustrated in Figure 6. The upper row of cropped panels shows streamlines approximately on half a period apart in time, with A_h lying in the range of 98 to 79 m^2 s^{-1} (corresponding to $Re = 204$ to 253, respectively).

As time progressed, a nonlinear transition occurred, where the wake axis first developed sinuous left to right fluctuations, far downstream near the tail of the wake. These disturbances propagated upstream until they arrived close to the island, providing an instability that destroyed the lateral symmetry of the flow near the island.

The instabilities quickly grew in amplitude, and shedding began, first occurring at a considerable distance downstream. By day 100 ($A_h = 59$ m^2 s^{-1}, corresponding to $Re = 339$), the flow finally settled to a classical oscillating von Karman vortex street (lower set of cropped panels in Figure 6) now spaced slightly less than one cycle apart with a period of 5.8 days. With island diameter $d = 50$ km, upstream velocity $V_o = 0.4$ m s^{-1}, and eddy-pair shedding frequency $N = 1/5.8$ day^{-1}, the Strouhal number $St = dN/V_o = 0.25$. The period of the eddy pair shedding cycle was $\sim 60\%$ of the period of the linear normal mode, in good agreement with the value of 62% reported by Schar and Smith (1993b). The eddy shedding mode persisted until the end of the simulation at day 120 (with $A_h = 44$ m^2 s^{-1}, corresponding to $Re = 450$).

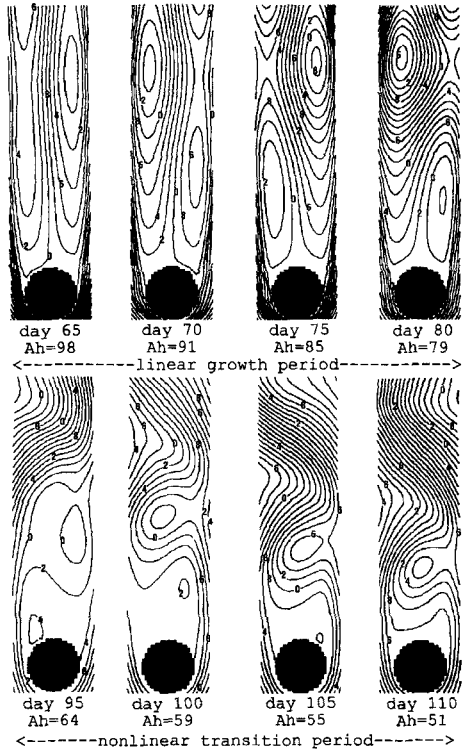

FIGURE 6 a) Streamfunction plots of a growing linear 10-day oscillating, but still attached, wake (top panels) [0, 1.6×10^5, 800 ($m^2\ s^{-1}$)], before developing into:
b) a 5.8 day von Karman vortex shedding wake (bottom panels) [0, 1.6×10^5, 1600 ($m^2\ s^{-1}$)]. The Reynolds number is given by $Re = 20{,}000/A_h$ ($m^2\ s^{-1}$), and was decreased very slowly during the runs to determine a critical value ($Re \sim 114$) for perturbations to appear in the wake and vortex shedding to develop.

The vertically integrated model was not run with varying bottom topography. Although such flows contain much interesting physics, in this paper we are primarily interested in surface intensified motions, such as are found in the ocean, and where the currents at great depth are likely to be insignificant (see Section 4.2).

4.1.2. Coriolis Force Effects

It is well known that Coriolis forces strongly affect three-dimensional flows (see Section 4.2). However, although they strongly affect pressure

in two-dimensional horizontal flows, for flat bottom topography, the equilibrated velocity field for non-rotating and f-plane flow around a vertical obstacle is identical.

Our two-dimensional model does not produce Stewartson layers, which are formed when bottom Ekman layers intersect a sidewall (Walker and Stewartson, 1972). Such layers can form in laboratory flows, however. Our intent was more focused on comparing results between simulations in an identical zero bottom stress regime with and without Coriolis forces present. So, as a check on the consistency of our model and to determine possible numerical effects due to truncation errors, we ran a series of cases both with no rotation and then for a f-plane ocean centered at Barbados (latitude = 13°10′N). The results showed that, as expected, rotation has only a very minor effect on the simulated two-dimensional velocity field after final steady state is attained (Dietrich *et al.*, 1994, Fig. 6). The difference between the maximum velocity inside the domain with and without the Coriolis terms was about 1 mm s^{-1} at 5.0 km horizontal resolution, and about 0.1 mm s^{-1} at 2.5 km resolution, both in the steady attached flow at low $Re = 39$, and in the vortex street cases at high $Re = 2000$. The rapid decrease of these differences with increasing resolution showed that it was due to truncation errors rather than being a direct result of the Coriolis terms.

Although the Coriolis terms vanish analytically for incompressible flow in the curl of the two-dimensional momentum equations, they vanish only to within truncation error in the corresponding finite difference curl of our model momentum equations. The interpolations used in evaluating the Coriolis terms lead to small Coriolis effects even though the velocity used is exactly divergence free before the interpolations. Although small interpolation errors lead to vorticity effects through the Coriolis terms, these errors do not lead to numerical instability, because the Coriolis term integration conserves energy except for purely dispersive interpolation effects. This is discussed further by Dietrich *et al.* (1994).

These small Coriolis terms truncation errors produce an interesting effect on the early stages of wake development. The model was restarted from rest, using a constant value of $A_h = 10$ $m^2 s^{-1}$ (corresponding to $Re = 2000$), both without and with Coriolis forces. Figure 7 shows the vorticity (upper panel), currents and pressure

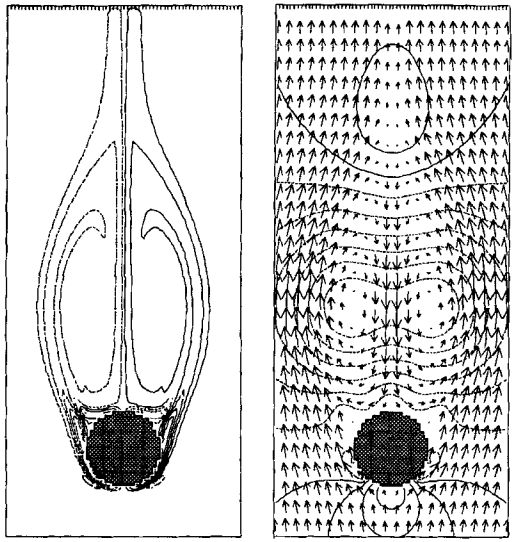

FIGURE 7 Results at day 40 in a non-rotating, high $Re = 2000$ run before the instabilities leading to eddy shedding have become significant.
a) vorticity [-105, 105, 19 (rad wk^{-1})];
b) velocity [max. speed 0.77 m s^{-1}] and pressure [0, 3.5, 0.32 (cm)]. Pressure units are in cm of water, which is the equivalent hydrostatic free-surface height anomaly.

(lower panel) at day 40 for a non-rotating ocean at 2.5 km resolution. The wake is perfectly symmetrical, and instabilities have yet to appear.

The situation is quite different for rotating flow. Figure 8 illustrates vorticity, currents and pressure also at day 40 and 2.5 km resolution, but with rotation ($f = 3.3 \times 10^{-5}$ s^{-1}) present. Coriolis-term truncation errors produce early finite amplitude perturbations leading to much earlier vortex street development. However, the equilibrated vortex streets found at a later stage (e.g., by day 100) are almost identical in both the non-rotating and rotating cases (see Dietrich *et al.*, 1994, Fig. 9), except the phase of the non-rotating wake leads the rotating wake by about one day.

The velocity vectors in Figure 7b show that the reverse currents directed back toward the cylinder along the wake axis entrain ambient flow into the vortex envelope. The strength of the reverse jet increases

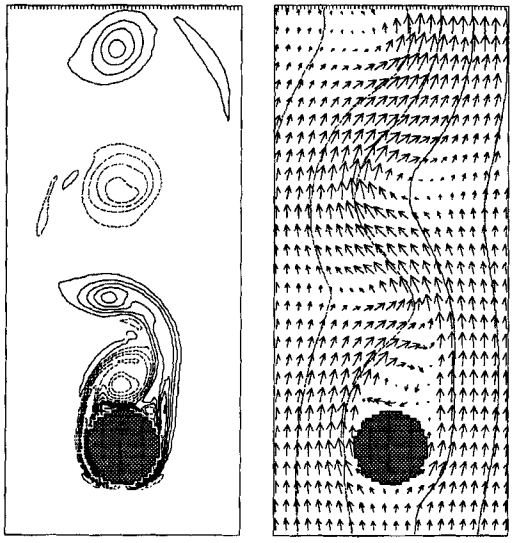

FIGURE 8 Results at day 40 in a rotating ($f = 3.31 \times 10^{-5}$ s^{-1}), high $Re = 2000$ run showing a well developed von Karman vortex street. These plots show how rotation leads to much earlier development of the vortex street as compared to the non-rotating case shown in Fig. 7.
a) vorticity [-122, 122, 21.4 (rad wk^{-1})];
b) velocity [max. speed 0.80 m s^{-1}] and pressure [0, 60.9, 5.5 (cm)]. Pressure units are in cm of water, which is the equivalent hydrostatic free-surface height anomaly.

with increasing Re. The jet splits at the central wake stagnation point just behind the island to produce significant counter-rotating vortices inside the wake envelope. These are associated with secondary side stagnation points (located at about 10 and 2 o'clock) where the counter-rotating vortices separate from the cylinder, in a very non-linear wake region. These vortices do not become significant until a critical Re is reached, and thus appear to be inherent features of the vortex street formation process described earlier.

The properties of the street are summarized in Table I for the rotating, two-dimensional, high $Re = 2000$ simulation. The flow patterns are quite similar in appearance to those created in the laboratory (e.g., Lin, 1954). The Strouhal number $St = dN/V_o = 0.25$, where N is the frequency of eddy-pair shedding, also lies centrally within the range of values reported for atmospheric vortex streets (0.15–0.32) by

TABLE I Summary of the mature wake characteristics for the rotating, two dimensional high $Re = 2000$ von Karman vortex street simulation (see Fig. 8).

Parameter	*Symbol*	*Value*
Island diameter	d	50 km
Speed of incident flow	V_o	0.4 m s^{-1}
Coriolis parameter	f	3.31×10^{-5} s^{-1} (13° 10' N)
Horizontal eddy viscosity	A_h	10 m^2 s^{-1}
Reynolds number	$Re = V_o d/A_h$	2000
Eddy pair shedding period	T_s	5.8 days
Eddy rotational period	T_r	2.5 days
Frequency of eddy pairs	$N = 1/T_s$	2.0×10^{-6} s^{-1}
Pitch (axial spacing)	a	125 km
Lateral spacing between rows	h	32 km
Aspect ratio	h/a	0.26
Eddy drift speed	V_e	0.26–0.35 m s^{-1}
Relative drift speed	V_e/V_o	0.65–0.88
Maximum eddy vorticity/f		1.80
Strouhal number	$S = dN/V_o$	0.25
Lin parameter	$B = S/Re$	1.25×10^{-4}

Atkinson (1981), but higher than the values of $St = 0.12$ found for the oceanic wake behind Johnston Atoll (Barkley, 1972), the $St = 0.16$ for the atmospheric street behind Madiera Island (Chopra and Hubert, 1965) and the $St = 0.17$ for the cyclones generated by Kahurangi Shoals (Bowman, *et al.*, 1983).

The geometry of our eddy field, as characterized by the ratio $h/a = 0.26$, where h is the lateral spacing between the two rows of vortices, and a is the axial spacing along each row, is very close to that predicted (0.28) for point vortices swirling in an inviscid fluid in a wake of infinite length (von Karman and Rubach, 1912).

It is interesting to note that the eddy rotational period $T_r = 2.5$ days is a little less than the gestation period of one eddy ($T_s/2 = 2.9$ days). This means that a particle introduced into the nearshore flow on one side of the island of a newly forming eddy will circulate once around before that eddy detaches.

The relative drift speed of the eddies as they are swept downstream by the ambient flow was 0.65 to 0.88, depending on distance downstream from the island, which lies in the range predicted by Chopra and Hubert (1964, 1965).

One difference in our results from Lin's (1954) observations is that our estimate of the Lin parameter $B = St/Re$ is smaller by an order of

magnitude than his. Lin's experiments produced recognizable von Karman vortex streets for only the very limited range $10^{-3} < B < 2.5 \times 10^{-3}$. In our simulations this is analogous to Re lying in the range $100 < Re < 250$; however we were able to produce stable von Karman vortex streets for at least the range $114 < Re < 2000$.

4.2. Three-Dimensional Flow Past a Steep Island

The three-dimensional simulations were patterned with topography, latitude, water column depth, stratification, and ambient flow conditions representative of Barbados. Hydrographic and current data were based on historical CTD and recent ADCP observations (Bowman *et al.*, 1994; Stansfield *et al.*, 1995). Possible influences of nearby topographic features on the island's wake were ignored. The most significant of these is the Martindale Seamount, located about 50 km north-north east of the island, and which rises to within 350 m of the sea surface (see Fig. 1).

The island topography was represented by an elliptical Gaussian bell with depth $h(x, y)$ (positive upwards) in meters given by

$$h(x, y) = 2200 \exp(-0.0008x^2 - 0.0004y^2) - 2000, \tag{2}$$

where x and y are distances measured in km to the "east" and "north" respectively from the center of the island (not true east and north; the reference frame was rotated 30° counterclockwise from true north to align the major axis with the ambient flow direction, which enters through the "southern" face of the box). This idealized representation has Barbados rising out of an abyssal plain of 2000 m depth, with the upper 200 m penetrating the ocean surface. The maximum bottom slope of about 5% occurs about 25–35 km from the center of the island at a depth of about 500 m below mean sea level (Fig. 9).

For efficiency, model densities were calculated from mean profiles of representative National Oceanographic Data Center (NODC) hydrographic data (Fig. 10), linearly relating density to temperature, holding salinity constant at 36.00 psu. The temperature profiles were all characterized by an upper mixed layer of 100 m with temperature ~ 26.5°C, overlying a sharp thermocline down to ~ 1000 m, and then a more

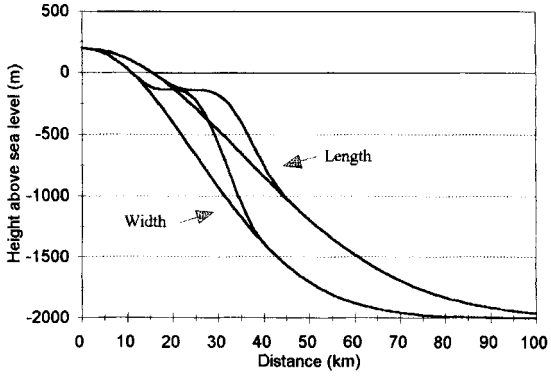

FIGURE 9 Elliptical Gaussian bell bathymetric profiles approximating the topography around Barbados (Fig. 1). The addition of the continental shelf around the island is also shown superimposed on the Gaussian bell.

gradual decline in temperature down to 2°C at 4000 m (the maximum model depth was 2000 m).

Salinity in the upper 50 m was quite variable, ranging from ~ 31 to 36.5 psu. This is a consequence of the frequent incursion of fragments of Amazon River water into the region (Stansfield *et al.*, 1995). The subsurface salinity maximum at 100 m is attributable to the northward transport and sinking of tropical surface water (Weyl, 1970). A broad salinity minimum centered around 800 m is Antarctic Intermediate Water. As mentioned above, the intent was not to reproduce these salinity features, but rather to use a representative density field based on the temperature profile for the baroclinic circulation.

The initial and inflow conditions were prescribed as follows. An inflow velocity distribution with representative vertical shear (as based on the ADCP observations) of the form $V(z) = 0.4\exp -(z/k)^2$ m s^{-1}, $(z < 0)$, with $k = 400$ m was first defined. A perturbation temperature was then derived from the thermal wind equation, and added to the background temperature, to give a geostrophically balanced inflow, constant at any given depth across the inflow channel. This temperature distribution was also used as climatology within the interior to initialize the flow. These inflow conditions were used for all three-dimensional runs except for those testing the effects of changing latitude (section 4.2.3).

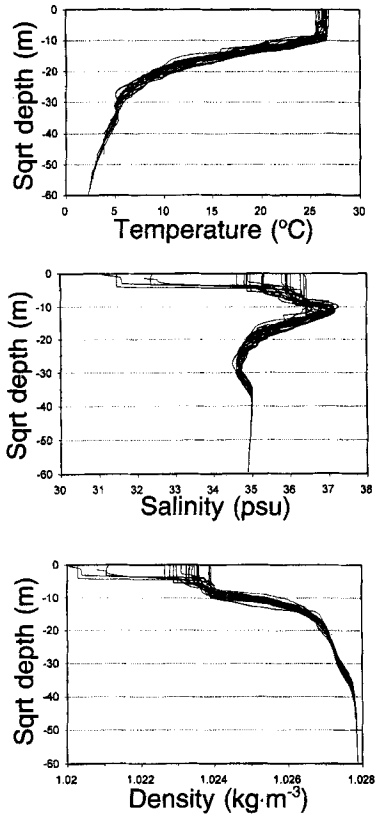

FIGURE 10 Composite plot of 21 hydrographic CTD profiles taken from the National Oceanographic Data Center archives for the seas adjacent to Barbados without regard to season. The vertical scale is the square root of depth to more conveniently display important features of the profile. a) temperature; b) salinity; c) density. The large scatter in surface salinity is due to the intrusion of Amazon River water into the region.

All boundaries were assumed thermally insulated. Wind stress was set to zero. The normalized botttom stress τ was parametrized as

$$\tau = -0.002\,\mathrm{V}\,|\mathrm{V}|\ \mathrm{cm}^2\,\mathrm{s}^{-2},$$

where V is the velocity in the cell closest to the bottom.

A stronger outflow constraint was used to minimize reflections of gravity waves in the three-dimensional runs. In a band of rows nearest the outflow, a simple relaxation towards the specified inflow profile

was used. The band was 1/8 of the total number of rows in the domain. The last interior zone takes 90% of the local value and 10% of the inflow value at each time step. The fraction of inflow value reduces linearly, row by row, from 10% down to zero at the upstream end of the band. This eliminates vortex stretching between the inflow and outflow, while virtually eliminating internal wave reflections.

The model was run with 10 levels in the vertical, with each cell increasing in thickness geometrically from 22 m at the surface to 640 m at the bottom. This maximized resolution near the surface where motions are intensified. The vertical eddy diffusivity used included a background value of 1 $cm^2\ s^{-1}$ plus an adjustment based on local turbulence. This adjustment is linearly related to a specified vertical cell Reynolds number ($Re_{cell} = w\Delta z/A_v$), where w is the local vertical velocity, Δz is the vertical grid interval, and A_v is the vertical eddy viscosity. The turbulence adjustment value was always less than 10 $cm^2\ s^{-1}$.

The horizontal eddy viscosity and thermal diffusivity were set equal, and were sufficiently small so that the resolved horizontal scales were always dominated by advection.

4.2.1. Elliptical Gaussian Bell Shaped Island: Effect of Viscosity

Figure 11 compares top layer (0–22) m) relative vorticity at day 90 from two cases, identical except for different values of horizontal eddy viscosity ($A_h = 2\ m^2\ s^{-1}$; left panel; $A_h = 10\ m^2\ s^{-1}$; right panel). The nearly identical results indicate that weak horizontal viscosity has little effect in vorticity generation compared to bottom drag on streams flowing over sloping topography. This implies that the difference between using lateral free-slip and no-slip conditions at the coast should be small. This was tested and found indeed to be true when realistically small A_h values were used.

4.2.2. Elliptical Island: Effect of Bathymetry Variation

The next case that we considered was identical to the higher horizontal viscosity case illustrated in Figure 11 (right panel: $A_h = 10\ m^2\ s^{-1}$), except that a 15 km wide continental shelf of approximate depth

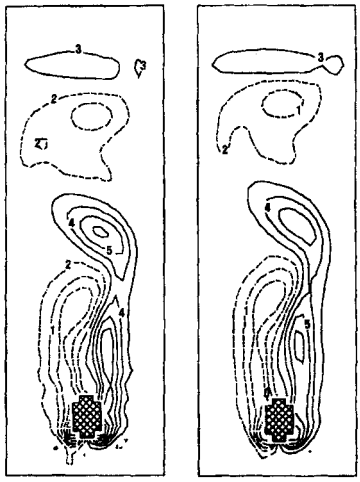

FIGURE 11 Contours of relative vorticity at day 90 in the surface layer (22 m) for the elliptical Gaussian bell shaped island, with Coriolis forces, stratification and upstream velocity set appropriate to Barbados. The two cases are identical except for horizontal viscosity.
a) $A_h = 2\ m^2\ s^{-1}$ (left panel) [−23.8, 24,4, 4.38 (rad wk^{-1})];
b) $A_h = 10\ m^2\ s^{-1}$ (right panel) [−25.9, 25.8, 4.70 (rad wk^{-1})].

100 m below sea level was added around the island (Figure 9). All parameters for both runs were the same except for island shape. Figure 12 compares surface (upper 22m) relative vorticity for an eight day period between days 92 and 100 from the Gaussian island-profile case (upper 5 panels) and the island-with-shelf case (lower 5 panels).

The presence of the shelf, while not significantly affecting the geometry of the wake eddies, did lead to a major increase in the eddy shedding period in the surface layer (upper 22 m) even though the island coastline shape was the same for the two cases at this level. The eddy shedding period changed from 8.25 days for the Gaussian profile island to 13.75 days after the shelf was added, an increase of 67%.

The maximum relative vorticity in the fully developed cyclonic lobes for the no-shelf case was about $2.5 \times 10^{-5}\ s^{-1}$ (numerically equal to $\sim 75\%$ of f). This was about 20% more than that for the shelf case. On the other hand, the vorticity in the no-shelf case was contained within an area which was somewhat less than that for the

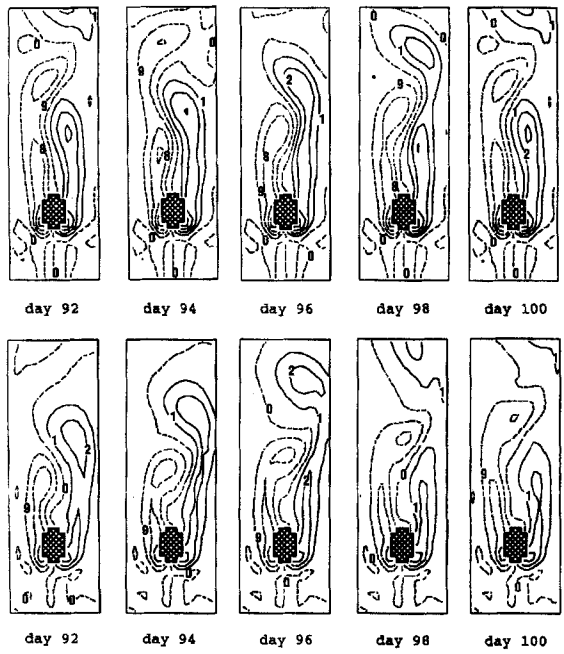

FIGURE 12 Comparison of relative vorticity in the surface layer (upper 22 m) for an eight day period between days 92 and 100 for the Gaussian bell island, with and without a continental shelf. The cases are identical except for the bathymetry adjustment. $A_h = 10\ m^2\ s^{-1}$.
a) upper five panels: island without shelf, shedding period 8.25 days [−24.0, 24.1, 4.38 (rad wk^{-1})];
b) lower five panels: island with shelf, shedding period 13.75 days [−20.2, 20.0, 3.65 (rad wk^{-1})].

shelf case. The circulation, defined by the vorticity integrated over the lobe area, turned out to be larger for the shelf case by about 15%. So, even though bottom torques were weaker, their influence over the larger surface area of the continental shelf more than compensated.

Relative vorticity contours beyond the shelf break, within the thermocline (330 m) are shown in Figure 13. In contrast to the eddy-shedding surface layer, the vorticity contours for both the no-shelf and shelf cases, while elongated in the along-flow direction, are almost time-invariant. Their shape is similar to the subcritical non-shedding

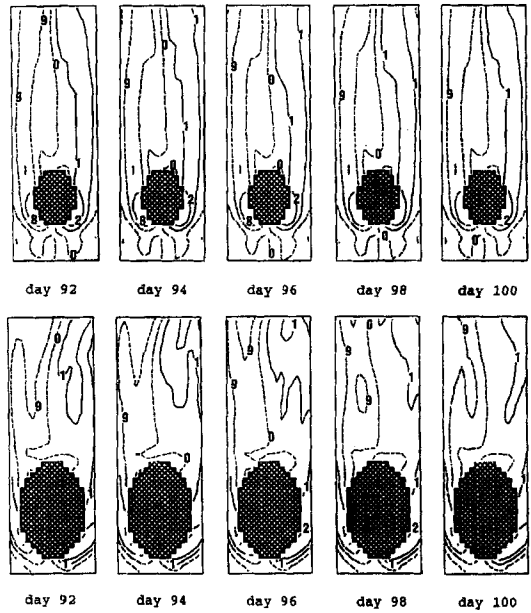

FIGURE 13 Comparison of relative vorticity in the thermocline (depth 330 m) for an eight day period between days 92 and 100 for the Gaussian bell island case with and without a continental shelf. The cases are identical except for the bathymetry adjustment. Eddy shedding has been suppressed at both levels. $A_h = 10\ \mathrm{m^2\ s^{-1}}$.
a) upper five panels: island without shelf [-15.8, 15.7, 2.86 (rad $\mathrm{wk^{-1}}$)];
b) lower five panels: island with shelf [-16.9, 15.6, 2.95 (rad $\mathrm{wk^{-1}}$)].

regime of the classical two-dimensional von Karman problem. This suggests that stratification coupled with lower mean velocities at depth have suppressed eddy shedding at this level. Thus we conclude that eddy shedding is highly surface intensified for the situations modeled.

Significant vertical motions occurred in the vicinity of the islands. The island-scale Rossby number $Ro = V_o/fr = 0.24$ (i.e., the Rossby number calculated using the island radius r at a given depth, here taken as $r = 25$ km) was generally significant, so the rotational constraint on vortex stretching was relatively weak. This can lead to locally large flows across depth contours, which can increase bottom drag when a current stream moves toward shallow water. Conver-

gence in shelf bottom waters leads to Ekman pumping; vertical motions of about +/− 10 meters per day and larger were common near the island and in its wake (see Dietrich *et al.*, 1994; Fig. 17). This can result in rather substantial changes to the density field.

Information about the vertical structure of the eddies can be deduced from horizontal sections of time-averaged temperature through the wake. Figure 14 shows horizontal slices of temperature at 10 m, 37 m, 75 m, 131 m, and 213 m for both the no-shelf case (upper five panels) and the shelf case (lower five panels). Maximum and minimum temperatures listed under the plots are for the entire domain, and not just the cropped panels shown. However, most of the deviations from

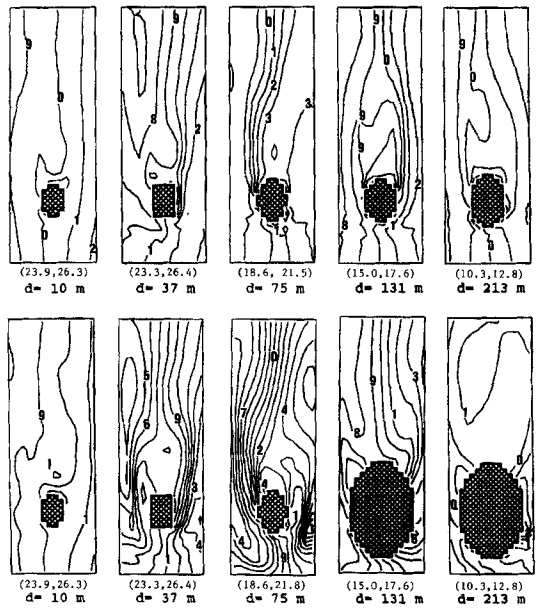

FIGURE 14 Comparison of time averaged temperatures at various depths for:
a) Gaussian bell island case (upper five panels);
b) island with shelf case (lower five panels). These plots show how eddy shedding has been suppressed at depth by stratification and decreased flow velocities, as evidenced by reduced horizontal temperature gradients (proportional to geostrophic velocities). Note the strong axial front that has developed along the left side of the wake (looking downstream) at 75 m (middle lower panel). Contour intervals are given by $(T_{max} - T_{min})/10$ °C. T_{max} and T_{min} are listed under each panel, and are the temperatures for the entire domain, not just the windows shown.

the mean geostrophic horizontal temperature gradient were confined to the wake, and so the values are representative of the disturbance created by the island.

For the no-shelf case, the maximum disturbance occurred at 37 m, with a horizontal temperature contrast of 3.1 °C measured across the domain, as compared to the 2.4 °C undisturbed background. For the shelf case, the maximum disturbance occurred mid-shelf at 75 m with a horizontal temperature contrast of 3.2 °C. In both cases, by 213 m the temperature gradient was almost back to ambient, illustrating that the baroclinic nature of the disturbances were concentrated within the upper water column. It is particularly worth noting that a strong shelf-break temperature front, best defined at 75 m (Fig. 14; middle lower panel), formed on the flanks of the island, and stretched several island diameters downstream, particularly on the left side of the wake.

4.2.3 Effects of Varying Latitude

An experiment was performed analogous to the higher viscosity case ($A_h = 10\ m^2\ s^{-1}$; Figure 12), except the Coriolis parameter was halved to $1.65 \times 10^{-5}\ s^{-1}$, a value appropriate for latitude 6.5 °N. The same initial hydrographic and inflow velocity structures were used, except the horizontal temperature gradients were reduced in order to maintain the thermal wind balance across the domain.

The eddy pair shedding period decreased from 8.25 to ~ 7.0 days, while at the same time vertical velocities within the eddy cores approximately doubled, with maximum upwelling of ~ 18 m day^{-1} located at a depth of ~ 265 m within cyclones, and similar maximum downwelling velocities at ~ 170 m within anticyclones. Thus, while the Coriolis forces have no effect on flat bottomed two-dimensional flows (see Section 4.1.2), they do have a significant effect on three-dimensional flows over sloping topography.

5. DISCUSSION

The Strouhal number is a useful way of summarizing the kinematic properties of the vortex street. It does not depend explicitly on either

horizontal or vertical viscosity, rotation or stratification, but only on the size of the island, the upstream velocity, and the geometry of its vortex street. The inverse of the Strouhal number can be thought of as approximating the spacing between successive cyclones (or anticyclones) in units of island diameter. For example, $St = 0.25$ implies that eddies of the same sense of rotation are spaced about 4 island diameters apart (actually it is less than this depending on the relative drift velocity of the eddy field to the ambient upstream velocity. For a relative drift speed of 75%, eddies would be spaced about 3 island diameters apart).

Table II summarizes the shedding periods T_s and the Strouhal numbers St estimated from our various experiments for fully developed vortex streets. The values of Re based on horizontal eddy viscosity are not reported for the 3D runs, since vertical viscosity over sloping topography is the more appropriate parameter.

For the 2D cylinder runs, the value of $St \sim 0.25$ depended neither on rotation nor Reynolds number in the range $Re = 114$–2000. The values of St estimated for the 3D island runs were about 50% of those calculated for the 2D simulations, and are similar to values reported from observations of both oceanic and atmospheric wakes behind islands (e.g., Chopra and Hubert, 1965; Barkley, 1972; Bowman, 1986) as well as recent numerical simulations (e.g., Schar and Smith, 1993b).

Although the presence of the continental shelf significantly increased the shedding period, the larger cross-section of the island meant that St remained almost constant at 0.13 at the latitude of

TABLE II Summary of eddy pair shedding periods T_s and Strouhal number St for the various experiments discussed in the text

Experiment	*Text section*	f $(10^{-5}s^{-1})$	d (km)	A_h (m^2s^{-1})	A_v (cm^2s^{-1})	Re	Ts $(days)$	St
2D cylinder ($f = 0$)	4.1.1	0	50	175–44	n/a	114–450	5.8	0.25
2D cylinder ($f = 0$)	4.1.1	0	50	10	n/a	2000	5.8	0.26
2D cylinder ($f > 0$)	4.1.2	3.31	50	10	n/a	2000	5.8	0.26
3D island (no shelf)	4.2.1	3.31	40	2,10	1–10	n/a	8.25	0.14
3D island (with shelf)	4.2.2	3.31	60	10	1–10	n/a	13.75	0.13
3D island (no shelf)	4.2.3	1.65	40	10	1–10	n/a	7.1	0.16

Barbados. Halving the Coriolis parameter for the no-shelf case caused a slight increase in *St* to 0.16, caused by a corresponding slight decrease in the shedding period. The effective diameter of the island is somewhat arbitrary, since the bottom slope is so small; we chose values of 40 km and 60 km for the no-shelf and with-shelf cases, respectively. The choice of an appropriate value of upstream velocity is also somewhat subjective; for example choosing a value of 0.2 m s^{-1} (found at 330 m below sea level) would raise the value of *St* to 0.25, commensurate with that found for the 2D vertical cylinder case.

The results in Section 4 show that three-dimensional effects are substantial in flows around islands modeled with realistic topography and stratification. Identical twin experiments have confirmed that the role of horizontal eddy viscosity is secondary compared to bottom drag in generating vorticity over sloping topography in shelf seas. The parameter that most affected the shedding period (an increase of 67%) was the addition of the continental shelf surrounding the island. Cutting the Coriolis parameter in half produced only a 14% drop in period.

Although the vorticity generation mechanism in the 3D simulations is fundamentally different to that in the 2D case, the advection of vorticity into a geometric, low dissipation, vortex street is essentially the same in both regimes, and helps explain their similar appearance. An accurate dynamical description of oceanic island wakes with realistic topography, stratification, vertical current shear and Coriolis forces requires fully three-dimensional modeling with low dissipation to properly understand the underlying physics.

For the island-with-shelf case, strong temperature fronts, with strongest horizontal gradients located at shelf-break depths were formed on the edges of the wake, and were particularly well formed along the left edge looking downstream. Near shore variations in cross-frontal temperature contrasts were much more nonlinear than the no-shelf case. Associated upwellings and downwellings can be important in local island ecosystems, e.g., the dispersal and retention of tropical reef fish larvae and juvenile fish (Cowen and Castro, 1994), as well as to the commercial fisheries, and the dispersal of wastes discharged at the coastline.

Acknowledgements

This research was supported by the Office of Naval Research's Navy Ocean Modeling and Prediction Program under contract N00014-92-J-4109 with Mississippi State University, and by the National Science Foundation under grants 0CE-8911120 to R.K. Cowen and M.J. Bowman, and grants OCE-8922124, OCE-9021904, and 0CE-9221756 to M.J. Bowman and S.J. Fauria. The use of the computational facilities at the Centre de Recherche en Calcul Applique (CERCA) in Montreal is gratefully acknowledged.

References

Aktinson, B. W. "Meso-scale Atmospheric Circulations", Ch 4, Academic Press, New York (1981).

Barkley, R. A. "Johnston Atoll's wake," *J. Mar. Res.* **30**, 201–216 (1972).

Batchelor, G. K. *An Introduction to Fluid Dynamics*, Cambridge University Press, Cambridge (1967).

Black, K. P. and Gay, S. L. "Eddy formation in unsteady flows," *J. Geophys. Res.* **92**, 9514–9522 (1987).

Bowman, M. J., Chiswell, S. M., LaPennas, P. L., Murtagh, R. A., Foster, B. A., Wilkinson, V. and Battaerd, W. "Coastal upwelling, cyclogenesis and squid fishing near Cape Farewell, New Zealand," in: *Coastal Oceanography* Eds. (Gade, H., Edwards, A., and Svendsen, H., 279–310, Plenum Press, NY (1983).

Bowman, M. J., Stansfield, K. S., Fauria, S. J. and Wilson, T. C. "Coastal ocean circulation around Barbados, West Indies, Spring 1990 and 1991," *J. Geophys. Res.* **99**, 16, 131–16, 142 (1994).

Boyer, D. L. "Flow past a right circular cylinder in a rotating frame," *J.Basic Eng.* **92**, 430–436 (1970).

Boyer, D. L. and Davies, P. A. "Flow past a circular cylinder on a Beta-plane," *Phil. Trans. R. Soc. Lond.* **A306**, 533–556 (1982).

Boyer, D. L. and Kmetz, M. L. "Vortex shedding in rotating flows," *Geophys. Astrophys. Fluid Dynam.* **26**, 51–83 (1983).

Brevdo, L. and Merkine, L. "Boundary layer separation of a two-layer rotating flow on a *f* plane," *Proc. R. Soc. Lond.* **A400**, 75–95 (1985).

Brighton, P. W. M. "Strongly stratified flow past three-dimensional obstacles," *Quart. J.R. Met. Soc.* **104**, 289–307 (1978).

Bryan, K. "A numerical method for the study of the circulation of the world ocean," *J. Comp. Phys.* **4**, 347–376 (1969).

Chapman, A. and Haidvogel, D.B. "Formation of Taylor caps over a tall, isolated seamount in a stratified ocean," *Geophys. Astrophys. Fluid Dynam.* **64**, 31–65 (1992).

Chiswell, S. M. "Vorticity and upwelling near an isolated topographic feature on the continental shelf", Ph.D. dissertation, Marine Sciences Research Center, State Univ. of New York, Stony Brook, NY pp. 203 (1993).

Chopra, K. P. "Atmospheric and oceanic flow problems introduced by islands," *Advances in Geophysics* **16**, Academic Press, New York, 297–421 (1973).

Chopra, K. P. and Hubert, L. F. "Karman vortex streets in earth's atmosphere," *Nature* **203**, 1341–1343 (1964).
Chopra, K. P. and Hubert, L. F. "Karman vortex streets in wakes of islands," *J. AIAA* **3**, 1941–1943 (1965).
Cowen, R. K. and Castro, L. R. "Relation of coral reef fish larval distributions to island scale circulation around Barbados, West Indies," *Bull. Mar. Sci.* **5**, 228–244 (1994).
Cox, M. "A primitive equation, three-dimensional model of the ocean, Geophysical Fluid Dynamics Laboratory", Ocean Group Technical Report No. 1, NOAA, Princeton, N.J., 143 (1984).
Davies, P. A. and Mofor, L. A. "Observations of flow by an isolated island," *Int. J. Remote Sensing* **11**, 767–782 (1990).
Deleersnijder, E., Wolanski, E., and Norro, A. "Numerical simulation of the three-dimensional tidal circulation is an island's wake," in: *Computers and experiments in fluid flow*, (Eds M. Carlomagno and C. A. Brebbia), *Computat. Mech. Pubs.*, Springer-Verlag, Berlin, pp. 355–381 (1989).
Deleersnijder, E. Norro, A. and Wolanski, E. "A three-dimensional model of the water circulation around an island in shallow water," *Cont. Shelf Res.* **12**, 891-906 (1992).
Denniss, T. and Middleton, J. H. "Effects of viscosity and bottom friction on recirculating flows," *J. Geophys. Res.* **99**, 10, 183–10, 192 (1994).
Dietrich, D. E. "A program of elliptic solver development and implementation in semi-implicit numerical ocean models, JAYCOR Final Report #J510-81-053-/2192", *Naval Ocean Research and Development Activity*, Stennis Space Center, MS. (1981).
Dietrich, D. E. *The Sandia Ocean Modeling System Programmers Guide and Users Manual*, SAND92-7386, Sandia National Laboratories, Albuquerque, NM (1992).
Dietrich, D. E., and Ko, D.-S. "A semi-collocated ocean model based on the SOMS approach," *Int. J. Num. Methoods in Fluids* **19**, 1103–1113 (1994).
Dietrich, D. E., and Lin, C. A. "Numerical studies of eddy shedding in the Gulf of Mexico", *J. Geophys. Res.* **99 (C4)**, 7599–7615 (1994).
Dietrich, D. E., Bowman, M. J. and Lin, C.A. Numerical studies of small island wakes, Tech. Report 94-1, Miss. State Univ. Center for Air Sea Technology, Stennis Space Center, MS, pp. 47 (1994).
Dietrich, D. E., Ko, D.-S. and Yeske, L. A., On the application and evaluation of the relocatable DieCAST ocean circulation model in coastal and semi-enclosed seas, Tech. Report 93-1, Center for Air Sea Technology, Miss. State Univ (1993).
Dietrich, D. E., Marietta, M. G. and Roache, P J. "An ocean modeling system with turbulent boundary layers and topography: numerical description," *International J. Num. in Fluids* **7**, 833–855 (1987).
Dietrich, D. E., McDonald, B. E. and Warn-Varnas, A. "Optimized block-implicit relaxation," *J. Comp. Phys.* **18**, 421–439 (1975).
Dietrich, D.E., Roache, P. J. and Marietta, M. J. "Convergence studies with the Sandia Ocean Modeling System," *Int. J. Num. Methods in Fluids* **11**, 127–150 (1990).
Dukowicz, J. K. and Malone, R. C. *Parallel Ocean General Circulation Modeling*, Technical Report LA-UR-92-200, Los Alamos National Laboratories, Los Alamos, NM (1992).
Falconer, R. A., Wolanski, E. and Mardapitta-Hadjipandeli, L. "Numerical simulation of secondary circulation in the lee of headlands," *Proc. Int. Conf. Coastal Eng. 19th* **(3)**, 2414–2433 (1985).
Falconer, R. A., Wolanski, E. and Mardapitta-Hadjipandeli, L. "Modelling tidal circulation in an island's wake," *J. Waterw., Port Coastal Ocean Eng. Div., Am. Soc. Civ. Eng.* **112 (2)**, 234–254 (1986a).
Falconer, R. A. and Mardapitta-Hadjipandeli, L. "Bathymetric and shear stress effects on an island's wake: a computational model study," *Coastal Eng.* **11**, 57–86 (1986b).
Fu, L-L. and Holt, B. "Seasat views oceans and sea ice with synthetic-aperture radar," *JPL publication* 81-120, JPL, Cal. Inst. Tech., Pasadena, CA (1982).

Heburn, G W., Kinder, T H., Allender, J. H. and Hurlburt, H. E. "A numerical model of eddy generation in the southeastern Caribbean Sea," in: *Hydrodynamics of Semi-enclosed Seas*, (Ed. J.C.J. Nihoul) 299–328, Elsevier, Amsterdam (1982).

Hogg, N. G. "Observations of internal Kelvin waves trapped around Bermuda," *J. Phys. Oceanogr.* **10**, 1353–1376 (1980) (1987).

Ingram, R. G. and Chu, V. H. "Flow around islands in Rupert Bay: an investigation of the bottom friction effect," *J. Geophys. Res.* **92**, 14,521–14, 533 (1987).

Kinder, T. H., Heburn, G. W. and Green, A. W. "Some aspects of the Caribbean circulation," *Marine Geology* **68**, 25–52 (1985).

Lin, C. C. "On periodically oscillating wakes in the Oseen approximation," in: *Studies in Mathematics and Mechanics*, presented to Richard von Mises, 170–176, Academic Press, NY, 353 pp. (1954).

Lugt, H. J. and Haussling, J. J. "Laminar flow past an abruptly accelerated elliptic cylinder at 45° incidence," *J. Fluid Mech.* **65**, 711–734 (1974).

Merkine, L. "Flow separation on a beta-plane," *J. Fluid Mech.* **99**, 399-409 (1980).

Merkine, L. "A linear analysis of rotating stratified flow past a circular cylinder on an f-plane," *J. Fluid Mech.* **157**, 501–518 (1985).

Merkine, L. and Solan, A. "The separation of flow past a cylinder in a rotating system," *J. Fluid Mech.* **92**, 381–392 (1979).

Middleton, J. H., Griffin, D. A. and Moore, A. H. "Oceanic circulation and turbulence in the coastal zone," *Const. Shelf Res.* **13**, 143–168 (1993).

Pattiaratchi, C. "Physical oceanographic aspects of the dispersal of coral spawn slicks: a review," in: *The Bio-Physics of Marine Larval Dispersal*, (Eds Sammarco, P. W. and Heron, M. L.) (1994) Coastal and Estuarine Studies no. 45, Am. Geophys. Union, Washington, D.C., 352 (1994).

Pattiaratchi, C., James, A. and Collins, M. "Island wakes and headland eddies: a comparison between remotely sensed data and laboratory experiments," *J. Geophys. Res.* **92**, 783–794 (1986).

Pingree, R. D. and Maddock, L. "The effect of bottom friction and Earth's rotation on an island's wake," *J. Marine Biol. Assn. U.K.* **60**, 499-508 (1980).

Roache, P. J. "Marching methods in elliptic equations," *Num. Heat Transfer* **1**, 1–201 (1978).

Schar, C. and Smith, R. B. "Shallow-water flow past isolated topography. Part I: vorticity production and wake formation," *J. Atmos. Sci.* **50**, 1373–1400 (1993a).

Schar, C. and Smith, R. B. "Shallow-water flow past isolated topography. Part II: transition to vortex shedding," *J. Atmos Sci.* **50**, 1401–1412 (1993b).

Signell, R. P. and Geyer, W. R. "Transient eddy formation around headlands," *J. Geophys, Res.* **96**, 2561–2575 (1991).

Smith, R. B. "Hydrostatic flow over mountains," *Advances in Geophysics* **31**, pp 1–41, Academic Press, NY (1989).

Stansfield, K. L., Bowman, M. J., Fauria, S. J., and Wilson, T. C. "Water mass and coastal current variability near Barbados, West Indies," *J. Geophys. Res.* **100 C12**, 24, 819–24, 830 (1995).

Taneda, S. "Experimental investigation of the wakes behind cylinders and plates at low Reynolds numbers," *J Phys. Soc. Japan* **11**, 302–307 (1956).

Tomczak, M. "Island wakes in deep and shallow water," *J. Geophys. Res.* **93**, 5153–5154 (1988).

von Karman, T. and Rubach, H. "Uber den Mechanismus des Flussigkeits und Luftwiderstandes," *Phys. Z.* **13**, 49–59 (1912).

von Riegels, "Zur Kritik des Hele-Shaw-Versuchs," *Z. Angew. Math. Mech.* **18**, 95–106 (1938).

Walker, D. A. and Stewartson, K. "The flow past a circular cylinder in a rotating frame," *J. Appl. Math. and Phys. (ZAMP)* **23**, 745–752 (1972).

Weyl, P. K. *Oceanography: An Introduction to the Marine Environment*, J. Wiley & Sons, New York (1970).
Wolanski, E. "Island wakes and internal tides in stratified shelf waters," *Ann. Geophysicae* **4B**, 425–440 (1986).
Wolanski, E. "Island wakes in shallow waters," *J. Geophys. Res.* **93**, 1335–1336 (1988).
Wolanski, E. and Hamner, W. M. "Topographically controlled fronts in the ocean and their biological influence," *Science* **241**, 177–181 (1988).
Wolanski, E., Imberger, J. and Heron, M. L. "Island wakes in shallow coastal waters," *J. Geophys. Res.* **89**, 10, 553–10, 569 (1984).
Zuur, E. A. H. and Dietrich, D. E. "The SOMS model and its application to Lake Neuchatel," *Aquatic Sci.* **52**, 115–129 (1990).

APPENDIX I: EFFECT OF THE "SWAMP LAYER" APPROXIMATION

To deal with the presence of land areas in our model, we use the "swamp layer" numerical approach described in Section 3. This produces a very brief initial transient with significant flow over the island which has little long term effects. We have verified this by applying an iterative version of our pressure solver algorithm which rapidly relaxes the flow over land to zero in a given time step, while maintaining exact incompressibility at each iteration. This new elliptic pressure algorithm properly treats incompressible flow around islands by using a regular geometry elliptic solver iteratively, as described in Appendix II.

We ran two cases, one using the "swamp layer" approach and the other using the more accurate iterative approach described in Appendix II. The results are quite different during the first few time steps, with differences in horizontal velocity as large as a few cm s^{-1} near the island upstream stagnation point. However, results from the two cases were virtually identical after the early transient, even after many von Karman-like eddies were shed. Thus, the initially significant perturbation due to the non-zero initial flow over land did not grow, but decayed as vortices were shed. The Reynolds number was about 1000 in this case. This also suggests that subgrid scale high frequency turbulent fluctuations might not have a large effect on island vortex shedding, thus favoring the predictability of such shedding.

APPENDIX II: SURFACE PRESSURE SOLUTION IN IRREGULAR DOMAINS USING AN ITERATIVE APPLICATION OF A REGULAR DOMAIN ELLIPTIC SOLVER

The surface pressure formulation we used was the same as in Dietrich *et al.* (1987) and Dietrich (1992); and is similar to that of Dukowicz and Malone (1992). However, we employed a modified solution algorithm that is better suited for vector and parallel computers in a domain with irregular boundaries and islands.

The model is started with a trial surface pressure, such as from the previous time step. The hydrostatic relation is then applied to derive the pressure everywhere below the surface. The momentum equations are then marched one time step. Next a first surface pressure correction is estimated using Dietrich's aforementioned original procedure except that the top model layer is extended over land, resulting in a regular domain for the elliptic pressure solver. Thus, as part of an iteration to the exact solution, water is assumed to exist in a thin layer over land in the model. The pressure correction is then applied to the flow, with the flow over land set to zero. This results in a non-zero divergence at the true water locations in the top level, but only along coastal boundaries. A second pressure correction is then calculated using Dietrich's procedure. When this new pressure correction is added to the result of the first iteration, the divergence is exactly zero everywhere once again, but there is now some flow over land. However, this flow is much smaller than in the results of the first iteration. Further iterations can be carried out until the desired level of accuracy is achieved. In summary, the procedure is as follows:

i) apply a regular geometry solver to get the first pressure correction;

ii) apply the pressure correction to get a non-divergent velocity;

iii) set the flow over land to zero;

iv) evaluate the residual divergent velocity error adjacent to the corrected land boundary points; if the residuals are sufficiently small, the solution procedure is complete;

v) solve for a pressure correction forced by the residuals, and return to step ii).

There is rapid convergence as the residuals are highly localized along irregular coastal boundaries. This procedure reduces greatly the non-vectorizable and non-parallelizable computation often required by general direct elliptic solvers, while achieving much faster convergence than most iterative solvers. The direct solver used here is an EVP method (Dietrich, 1981; Roache, 1978) which fully vectorizes or parallelizes in one of the two dimensions. This procedure is similar to the "block implicit relaxation" methods used by Dietrich *et al.* (1975) for elliptic problems. Both are similar to domain decomposition methods and can be combined in application to large problems.